Laboratori Nazionali di Frascati

LNF–10/08 (P)
March 3, 2010

INFRARED AND X-RAY SIMULTANEOUS SPECTROSCOPY: A NOVEL CONCEPTUAL BEAMLINE DESIGN FOR TIME RESOLVED EXPERIMENTS

Augusto Marcelli[1], Wei Xu[2], Dariush Hampai[1], Luca Malfatti[3], Plinio Innocenzi[3], Ulrich Schade[4], and Ziyu Wu[2,5]

[1)] *INFN- Laboratori Nazionali di Frascati, Via E. Fermi 40, 00044 Frascati, Rome (Italy)*
[2)] *BSRF, Institute of High Energy Physics, Chinese Academy of Science, Beijing 100049, China*
[3)] *Laboratorio di Scienza dei Materiali e Nanotecnologie, Università di Sassari, D.A.P., CR-INSTM, Palazzo Pou Salit, Piazza Duomo 6, 07041 Alghero, Sassari (Italy)*
[4)] *Helmholtz-Zentrum Berlin für Materialien und Energie GmbH Elektronenspeicherring - BESSY II Albert-Einstein-Strasse 15 D-12489 Berlin (Germany)*
[5)] *NSRL, University of Science and Technology of China, Hefei 230026, China*

Abstract

Many physical/chemical processes such as metal-insulator transitions or self-assembly phenomena involve correlated changes of electronic and atomic structure in a wide time range from microseconds to minutes. To investigate these dynamical processes we not only need a highly brilliance photon source in order to achieve high spatial and time resolution but new experimental methods have to be implemented. Here we present a new optical layout to perform simultaneous or concurrent Infrared and X-ray measurements. This approach may indeed return unique information such as the interplay between structural changes and chemical processes occurring in the investigated sample. A beamline combining two X-ray and IR beams may really take advantage of the unique synchrotron radiation properties: the high brilliance and the broad spectrum. In this contribution we will describe the conceptual layout and the expected performance of a complex system designed to collect IR and X-ray radiation from the same bending magnet on a third generation synchrotron radiation ring. If realized, this beamline will allow time resolved spectroscopy experiments offering new scientific opportunities in many frontier researches.

PACS.: *07.85.Qe, 61.05.cj, 07.57.Ty, 78.47.jc*

Submitted to Analytical and Bioanalytical Chemistry (2010)

Servizio Informazione e Documentazione Scientifica dei LNF
Ufficio Biblioteca e Pubblicazioni

INTRODUCTION

More then 50 storage rings are now operational around the world and in almost all of these facilities the state-of-the-art of spectroscopic and scattering techniques are available with both linear and circular polarizations. Many physical/chemical processes such as metal-insulator transitions, self-assembly phenomena, structural ordering mechanisms, catalysis, etc., involving correlated changes of electronic and atomic structure can be investigated with the available instruments in the time domain. With the continuous improvement of the stability of the synchrotron radiation sources, of the instrumentations and of the detectors all experimental techniques allow exploiting the time domain down to the ms regime and in special case at even shorter time [1)]. Nevertheless, due to the complexity of the phenomena, the concurrent combination of an Infrared and X-ray simultaneous spectroscopic analysis may return unique information, e.g., the interplay between structural changes and chemical processes. As an example pioneering time resolved experiments combining X-ray and IR radiation were performed at Daresbury more than a decade ago [2)] and recently these experiments were improved combining at Elettra a x-ray beam with IR light emitted by a conventional source [3)].

Nowadays the combination of experimental techniques is a trend for many scientific cases [4)] and the strategy of a concurrent analysis is mandatory in frontier multi-disciplinary areas. Among the many techniques implemented in the synchrotron radiation facilities all around the world, the X-ray absorption spectroscopy [5)] (XAS) is certainly one of the most diffused techniques among synchrotron radiation users. XAS may be used to investigate the local structure in ordered and disordered systems and may identify subtle structural distortions or to characterize partial and local electronic properties by comparison among experimental data and the state-of-the-art *ab initio* calculations [6)]. Although suggested for the first time in 1966 [7)] and then in the early 70's [8)] and 80's [9)] in the USA, the use of IR Synchrotron Radiation (IRSR), contrary to XAS spectroscopy and due to many technical reasons, developed at a low rate. In particular, this has been due to the spectacular development of synchrotron radiation in the UV and X-ray domain, because of the lack of intense and brilliant sources in these energy ranges. Only at the beginning of the 80's, a port dedicated to the extraction of Infrared Synchrotron Radiation (IRSR) was built on the SRS ring at Daresbury by Yarwood [10)]. One of the young member of the original Daresbury team, Takao Nanba, coming back in Japan in 1985 started the construction on the UVSOR ring, one of the first synchrotron radiation dedicated rings, of the first IRSR beamline that later opened to users [11,12)]. Nowadays IRSR is growing at a fast rate and the increasing demand of new beamlines emerges in the most industrialized countries. What are the main reasons of the success of the infrared synchrotron radiation in these last years? Actually, in the infrared region the energy of the electron beam (for E>0.5 GeV) does not affect the synchrotron radiation spectral distribution, while the flux is proportional to the current circulating in a storage ring. As a consequence the infrared emission has the same shape for all storage rings and, current and stability which both increased significantly in these last years represent the qualifying parameters of an IR synchrotron radiation source. After UVSOR at Okazaki and NSLS at Brookhaven all around the world other IR beamlines were built and nowadays there are about 20 dedicated IRSR beamlines in the world in a context of continuously growing interest in various

areas, such as condensed matter physics, chemistry, biology, etc. and in particular for infrared spectromicroscopy.

Based on the large photon flux and brilliance in the X-ray region and on the high brilliance in the IR region, a synchrotron radiation facility represents for a scientist the ideal facility to perform X-ray or infrared spectroscopic/microscopic experiments. As was discussed in Ref. 4, the dynamic of many physical/chemical processes such as phase transitions and self-assembly processes, order/disorder phenomena, nano-systems or processes affected by a low dimensionality, surfaces and interfaces processes, unfolding processes of (metallo-)proteins and radiation damage or radiation resistance phenomena, can be studied by these two techniques with a concurrent approach on a short time scale (~ms). If a process or a reaction is reversible and reproducible, researchers can be reasonably performed with independent measurements on two separate and optimized beamlines. However, sometime samples do not survive to experiments and can not be used twice being many physical/chemical reactions irreversible. Moreover, in many case it is almost impossible to superimpose in the time domain two spectral behaviors collected independently in the X-ray and IR range with different time resolutions, in order to resolve changes associated to electronic, structural and/or vibrational contributions.

To meet this specific demand and to exploit the sub-ms time domain we recently proposed [13] a new conceptual layout combining infrared and X-ray beams collected from the same synchrotron radiation source. The main features of such complex beamline thought for time-resolved concurrent/simultaneous experiments are:

a) two X-ray and IR branches with their front-ends on the same bending magnet;
b) X-ray and Infrared beams transported separately with different optical systems merging at the end in the same optical hutch;
c) a unique experimental end station for both X-ray and IR with the two beams running in a paraxial geometry on the sample;
d) to fulfill the item c) the X-ray branch is an energy dispersive system coupled to a fast Position Sensitive Detector (PSD) [14,15] ideal for time-resolved XAS experiments;
e) a new optical spectrometer for the IR branch to allow faster acquisition respect to standard FTIR interferometer whose time resolution in rapid scan mode is limited to few ms.

In this contribution, we will present the conceptual design of the beamline tailored with the parameters of the SSRF source [16], one of the new third generation synchrotron radiation facilities and the largest one commissioned and operative in China.

The manuscript is organized as follows: in section 1 we compare the photon flux and the energy range of reference synchrotron radiation facilities; in section 2 we discuss the front end and technical issues associated to the extraction of IR and X-ray radiation from the same bending magnet; in section 3 we present the complete layout of a possible IR and X-ray Simultaneous Spectroscopy (IXSS) beamline, discussing the alignment issue and to make possible a paraxial geometry for both IR and X-ray beams through the sample. Finally in section 4 we will resume some expected performances of the beamline then a few conclusions are summarized.

BEAMLINE DESIGNING

1) Source

Regarding source parameters, one of the main parameter to be considered for the design of a concurrent beamline is the available photon flux both in the IR and X-ray domain. In Fig.1 we show a comparison of the photon flux of three light sources: two 3rd generation light sources such as SSRF [16] and Diamond [17] and BSRF [18] that is medium energy 2nd generation light source. To perform the comparison we selected the same horizontal collection angles for the three accelerators but different in the IR and in the X-ray range, i.e., 40 mrad and 4 mrad, respectively. Because they have different electron energies and a different vertical emission angle we selected different vertical opening angles, however suitable to collect for each source the entire emission. The complete list of parameters is in Table.1. Using the XOP package [19] the IR photon flux was calculated from 100 cm^{-1} (100 μm) up to 2000 cm^{-1} (5 μm) while in the X-ray domain from 5 to 35 keV. As shown in Fig.1, the photon flux increases linearly from 10^{13} to 10^{14} photon/sec/0.1% b.w. as the wavelength goes from the far-IR to the mid-IR being comparable to those available at SOLEIL (4×10^{13}@100μm) where two IR beamlines are operative in the far-IR and mid-IR [20]. Although SSRF shows the higher emission in the IR domain, the photon flux of the three sources is almost equivalent. On the contrary, in the X-ray domain, SSRF and Diamond deliver the higher photon flux, i.e., from 10^{12} to 10^{14} photon/sec/0.1b.w.% in a broad range from 5 to 35 keV while BSRF has a comparable flux only below 10 keV. According to these values a suitable conbination with IR and X-ray fluxes is still possible in a 2nd generation facility like BSRF only for E<10 keV, while an ideal beamline covering a wider energy range is feasible at 3rd generation facilities such as SSRF or Diamond.

2) The front end for the extraction of two IR&X-ray beams from the same bending magnet

To extract IR and X-ray radiation from the same bending magnet two separate ports have to be considered and we need to take in consideration the geometrical location of each ports. As showed in Fig.2, the separation between the two ports depends by

1) the divergence of the two photon beams or in alternative the maximum available aperture;
2) the angular distance between the two extraction ports on the storage ring arc;
3) the (minimum) distance from the bending magnet to the front end exit flanges.

Considering the standard size of CF flanges at SSRF at 1 m from the emission point on the bending magnet a standard CF63 (2.75”) flange can be used for the X-ray beam and a CF100 (6”) for the wider IR beam. With a simple geometrical calculation, we may obtain the minimum angle between the IXSS-IR and the IXSS-X sources, i.e., 8.95° corresponding to the arc of the SSRF bending magnet to a separation of 1.43 m. As the X-ray exit port, also the exit flange of the IR beam is located at 1 m from the IR source on the bending magnet. Taking into account the horizontal and vertical divergences, to transport both IR and X-ray beam without loss and avoiding the mechanical overlap and conflicts, two stainless steel pipes of a diameter 150 mm and 35 mm, respectively can be considered.

3) IXSS beam-line layout

As briefly outlined above the IXSS beamline can be thought as two independent optical systems that merge at the end. Therefore the beamline design is done separately for the first part upstream the experimental region where the sample is located. For the sample region a specific optical system and instruments have to be designed and realized.

The ray-tracing SHADOW VUI module in the XOP package [19] was used to optimize optics and estimate performance for the IR and X-ray optical systems. While X-rays can be deflected and/or focused using only long mirrors working at grazing incidence, the IR radiation can be easily deflected by mirrors working also at large incidence angles. As a consequence the IR beam path can be based on suitable reflecting optics and we may consider the alignment of the IR beam to the X-ray beam path. To achieve this result the ZEMAX^{TM} package [21] was used to perform the ray-tracing of the final converging optical system. In the next section, we will describe the basic optical elements and the layout of the X-ray and IR optical systems before to present the concept of the optical system that will allow merging the two beams to obtain a paraxial geometry at the sample location.

3.1) The IXSS x-ray branch

The IXSS-X layout is substantially an energy dispersive beamline with a crystal bent in the horizontal plane. A polychromatic beam is focused at the sample position by the bent crystal and the spectrum is collected in transmission by a position-sensitive detector placed at the right distance from the sample. Every pixel of the detector measure a different energy and with this dispersive geometry time-resolved spectroscopy is possible down to the micro-sec domain with an intense flux and stable beam [14]. The layout contains three main optical elements: two mirrors and one crystal. A cylindrical (possibly elliptical) focusing mirror M_{x1} with a demagnification factor of 0.8 is used to focus the beam in the vertical. The following plane mirror M_{x2} deflect the beam to a direction parallel to the storage ring plane avoiding radiation going upwards after the M_{x1} mirror. An elliptically bent crystal is the heart of this layout. The bent crystal disperses X-rays in the horizontal plane and focuses the polychromatic beam on the sample location.

The layout of X-ray branch is shown in Fig.3 and the corresponding optical parameters are listed in Table.3. In more detail, M_{x1} is a Pt coated plane mirror working at the glancing angle of 2.3 mrad that focuses the the X-ray beam in the vertical direction. As shown in Fig.5, the reflectivity of a Pt coated mirror remains above 75% in the entire energy range of interest around the optimized energy of 15 keV for the beam-line. Two slits inserted before the M_{x1} mirror and the bent crystal, confine and collimate respectively, the X-ray beam in the vertical and in the horizontal planes, respectively.

Using the kinetic theory, we may successfully calculate the properties of a flat crystal such as its angular distribution (rocking curve) and energy distribution (energy resolution). On the contrary, for a bent crystal the dynamical theory has to be considered to describe diffraction effects [15]. Indeed, when a crystal is bent, the lattice is distorted and therefore the interference between parallel lattice planes is partially destroyed and diffraction phenomena may occur. The dynamical theory may be used to calculate the reflectivity of a bent crystal on the basis of the

kinetic theory of mosaic model calculations. In this case, dynamical effects are introduced as correction factors like the primary or the secondary extinction. A detailed theory about bent crystals is available in Ref. 15 and in references therein.

To guarantee that the crystal collects all photons emitted by the source, we need a bent crystal whose length (L) depends by the crystal angular acceptance (δ), the source-crystal distance (p) and the Bragg angle θ_0

$$L = \frac{p\delta}{\sin\theta_0} \tag{1}$$

Actually, the effective length is limited also by the rocking curve of the bent crystal, within which the energy can be diffracted. The band pass of a bent crystal in the Bragg geometry can be calculated in the tangential focusing geometry (i.e., focusing in the plane of the scattering)

$$\frac{1}{p} + \frac{1}{q} = \frac{2}{R_t \sin\theta_0} \tag{2}$$

using the formula for the energy band pass of a cylindrically bent crystal

$$\Delta E = E_0 \cot\theta_0 2\delta \left(\frac{r}{2f} - 1\right) \tag{3}$$

where E_0 is the central energy, θ_0 is the Bragg angle, δ is the divergence of the source, r is the bent radius for the crystal and f is the focal length [22]. Using the Eq. 3 we list in Table.2 the values of a 0.7 mm thick Si(111) crystal at different energies. Considering the length of two bending magnet beamlines at SSRF, i.e. the BL14B (Diffraction) and the BL16B1 (Small angle scattering) that are 46 and 49 m long we hypothesized a source distance of 45 m and a detector distance of 2 m. The rocking curve calculation was performed with the XOP package [19] with an energy band pass of about 1000 eV at the Ti *K*-edge, the typical range for an EXAFS analysis. However, at energies greater than 20 keV, the diffraction curve exhibits fringes around the primary peak (Fig.5) pointing out a worsening of the crystal performance.

As pointed out above, the length of the Si crystal has to be calculated to collect the entire flux available from 4 mrad horizontal source divergence. However, a bent crystals with suitable performances may have a length of about 300 mm and!±2μm thickness homogeneity [14] while the ideal length of our bent crystal (Table.2) has to be much longer, i.e., L=0.91 m at 10 keV. In order to reduce its length we may introduce other mirrors and/or slits before the crystal, reducing the divergence of the X-ray beam, still collecting a large incident flux.

3.2) The IXSS infrared branch

The IXSS-IR optical system transports an infrared collimated beam to the final converging optical system: a concentrator that condenses the collimated beam increasing the photon density in the final spot. The first section of the beamline layout is a conventional IR layout. The optical elements of the IR branch are outlined in Fig.4 and the optical parameters are listed in Table.4. The main optical elements are:

1) the plane mirror M_{IR1} tilted by 45° in the vertical plane that extracts the IR radiation;
2) the toroidal mirror M_{IR2} used to focus the IR beam to the diamond window;
3) two spherical mirrors M_{IR3} and M_{IR4} (set below M_3) to collimate the beam in the horizontal and vertical directions, respectively;
4) the plane mirror M_{IR5} used as the steering element to align the IR beam along the same direction of X-rays;
5) the concentrator M_{IR6} that condenses the IR radiation in a small spot increasing the photon density.

3.3) Alignment issues

To perform time-resolved experiments, both source stability [23] and alignment of the X-ray and IR beams are critical issues. The alignment of the individual IR and X-ray optical systems need to be carefully considered. In the X-ray layout of the IXSS beamline, the vertical focusing mirror raises the beam up to $L/(2*\tan\theta)$, where L is the half-length of the mirror and θ is the grazing angle of the X-ray beam. The reflection of X-rays is mainly determined by both the atomic mass of the mirror surface and the grazing angle [24,25]. The critical angle for the total reflection is then determined by the coating materials and by the photon wavelength. Above the critical angle, the beam is totally reflected and a negligible photon loss occurs. Critical angles are quite small (a few mrad) mainly due to the short wavelength (~Å) of X-rays also using high Z coatings such as gold or platinum.

As it is shown in Fig.7, the IR mirrors M_{IR1} and M_{IR2} deflect the beam vertically by 77 cm above the storage ring while M_{IR3} and M_{IR4} deflect the beam downwards about 2 cm above the storage ring, where the X-ray beam travels. Because the bent crystal deflect the X-ray beam by $2\theta_B$, where θ_B is the Bragg angle for the central energy, the IR beam has to be adjusted to the X-ray path at each energy with two mirrors: the M_{IR5} working along the X axis deflects the IR radiation to the X-ray path while the following one M_{IR6} i.e., the condensing system (we will discuss details later) that generates an IR beam paraxial to the X-ray beam. The Bragg angles for the Si (111) crystal at different energies listed in Table.2 can be obtained with simple geometric calculations (Fig.7). In this layout, before the M_{IR6} mirror the IR path is maintained perpendicular to the X-ray beam moving the M_{IR5} along the x axis; while the distance between the centre of the bent crystal (BC) and the centre of M_{IR6} is arbitrarily set to 1 m (this space is that necessary to host the large condenser lens M_{IR6}). At low energy the Bragg angle increases and large deflection angles are necessary for the IR beam. At 5 keV (θ_B=23.3°) the IR beam has to be deflected by 136.4° while at 35 keV (θ_B=3.2°) the deflection angle is 96.2°. The analysis showing the space required and the parameters to design the required mechanical system to align the optical systems is described in Fig.8. This figure shows the positions of the M_{IR5} and M_{IR6} mirrors and the distance between them as function of the energy. The x and y coordinate of M_{IR6} increases as the X-ray energy increases. In Fig. 9 we show the curves of the positions of the two IR mirrors. Actually while M_{IR5} departs from the light source the distance between M_{IR5} and M_{IR6} rapidly increases going to low energy while above 10 keV it approaches the asymptotic value of ~7 m.

3.4) Beam convergence

To illustrate the principles of the condenser system (CS) that allows merging of the IR radiation with X-rays before the sample position we selected the energy of 15 keV. According to above, the key parameters are:

1) the size of the collimated beam at the entrance of the CS that is 15 (H) * 14 (V) cm;
2) the expected output size of the collimated beam set to ~0.3x0.3 mm^2;
3) the angle between the incident and the output beams set to 90°;
4) the distance between the centre of the condenser system and the centre of the bent crystal set to 1 m.

The cylinder-like condenser system has a diameter >150 mm and a length >5.3 m along the IR path. Considering the layout of Fig.10 for sake of clarity the coordinate system has been rotated to make it clearer, the system is a Schwarzschild-like system with five optical elements:

1) a primary gold coated mirror made by two parabolic segments (C_1 and C_2) separated by 0.3 mm along the vertical axis;
2) a secondary gold coated mirror made by other two parabolic segments (C_3 and C_4) glued together;
3) a partially transmitting plane mirror C_5 that allows the transmission of X-ray .

The ZEMAX™ package [21] has been used to ray-trace this complex optical layout. The focal lengths of the parabolic mirrors are 5090 mm and 10 mm for the primary and the secondary mirror, respectively. The mirrors C_1 and C_3 have a common focal point (or foci) while the mirrors C_2 and C_4 have one common foci. The two foci are separated by 0.3 mm in the vertical plane. All optical parameters are listed in Fig.10.

EXPECTED PERFORMANCES

The estimated monochromatic flux at 15 keV at SSRF is $4.8x10^{13}$ photon/s/0.1b.w. After the first two mirrors, the flux decreases to about 10^{12} photon/sec/0.1 b.w. The detector after the bent crystal always at 15 keV may count about $1.2*10^{10}$ photon/sec/0.1 b.w within an area of 80 μm (H) * 200 μm (V). Additional losses due to the condenser system are estimated < 5%.

Ray-tracing by SHADOW calculated the infrared source at 10 μm and accounted for photon losses due to two mechanisms: the reflectivity of gold mirrors and the absorption of the diamond window set between M_{IR2} and M_{IR3} whose effect is estimated to be about 30%. Taking into account both contributions the IR flux at the sample position is about $1.8\ x10^{14}$ photon/sec/0.1b.w at the wavelength of 10 μm within a spot of 300 * 300 μm^2.

Due to energy-dispersive geometry the detection of X-ray after the sample requires a position-sensitive detector [14,15]. A recently developed *Fine Pitch Germanium Microstrip Detector* [26] is a good candidate for our X-ray layout. The X-ray beam is focused on the sample by the bent crystal therefore the detector should be placed ~1 m away from the focal point (sample position) to optimize the energy resolution and to guarantee a reasonable space for the instrumental setup. For the IR detection, well established Mercury-Cadmium-Telluride (MCT) detectors and the recently developed MCT Focal Plane Array (FPA) can be considered [27].

Additional important evaluations of beamline performances concern:
1) the brilliance at the sample position, i.e., the integrated flux/sec within one steradian, the unit of the solid angle within a unit of the sample area, and
2) the acquisition time, i.e., the minimum time required to achieve a reasonable S/N ratio to collect a spectrum.

To optimize IXSS we have to optimize performances of both X-ray and the IR optical systems. Because of the high intensity of conventional source, to evaluate the advantage of the synchrotron radiation IR emission [28], we have to compare a SR source with a conventional Globar source in the mid-IR domain (400-4000 cm^{-1}) and a Hg lamp for the far-IR (40-400 cm^{-1}) range.

A Globar is substantially a black body source whose emission power is a function of the temperature of the emitter. Using the XOP package [19], the flux of a blackbody, with $1mm^2$ source area and 1mrad(H) * 1mrad(V) angular divergence, can be calculated (see Fig.11). The maximum flux and the wave-number is listed in Table 5 for different temperatures. The peak wave-number vs. flux at different temperatures is listed in Table 5. If we consider a thermal source working at 1800 K, the corresponding IR flux at 1000 cm^{-1} (10 μm) is $\sim 7*10^6$ photon/sec/0.1%b.w. As estimated by SHADOW, the available flux of IXSS at the wavelength of 10 μm within a sample area of 250 μm (H)*250 μm (V) is $1.5*10^{13}$ photon/sec/0.1%b.w. To perform IR experiment, the photon brilliance is more important than the flux. Dividing the photon flux by the source area and the solid angle, the brilliance available with the IXSS layout is $\sim 8.75*10^{15}$ photon/sec/mm^2/rad^2/0.1%b.w. at 10μm. At the same wavelength the photon brilliance of a 1800 K blackbody emission is $\sim 7*10^{12}$ photon/sec/mm^2/rad^2/0.1% b.w., three orders of magnitude lower than the SR emission.

Dispersive spectrometers associated to the modern focal plane technology can provide a tremendous benefit in terms of signal-to noise ratio (SNR) ratio and achievable time-resolution thanks to the high brilliance of the IR synchrotron radiation sources. The development of such spectrometers will probably introduce a paradigmatic change since up to now only commercially available Fourier Transform spectrometers (FTS) are used at IR beamlines. We propose here for the IXSS beamline a time-resolved grating spectrometer based on a customized linear Focal Plane Array (FPA) and a set of interchangeable gratings, covering the mid-IR spectral range. The design goals are shown in Table. 6. In particular, as an example, three different gratings coupled to a linear array of 256 pixels will be sufficient to cover the biologically interesting spectral areas around 3000 cm^{-1} (lipids), 1600 cm^{-1} (proteins) and 1000 cm^{-1} (carbohydrates). Generally, the aimed spectral resolution of 2 cm^{-1} is sufficient for most of the spectroscopic applications in life and materials science.

The spectrometer we consider has an entrance aperture which in contrast to a Globar source will almost be completely filled by the diffraction-limited infrared spot of the SR emission of the beamline. The area of the FPA detector pixel will then be used as an exit slit. The optical elements will be cooled at 77 K to minimize the thermal background radiation that degrades the performance of the spectrometer. The data typical for an 800 cm^{-1} cut-off array detector based on the ternary alloy mercury-cadmium-telluride (MCT) are given in Table. 7.

The SNR of such a spectrometer can be calculated from the different flux contributions picked up by the detector pixel according to:

$$SNR = \frac{\tau_{\text{int}}\,\eta\,\Phi_{\Delta\nu}}{\sqrt{\tau_{\text{int}}(\eta\,\Phi_{\Delta\nu} + \eta\,\Phi_{BG} + I_{dark})} + n_{RN}}, \qquad (4)$$

with τ_{int} - the integration time of the detector, η - the efficiency of the detector to convert photons into electrons, $\Phi_{\Delta\nu}$ - the spectral radian flux onto the detector pixel to be measured, Φ_{BG} - the radiant flux from the background falling into the field of view of the detector and for the spectral band the detector is sensitive, I_{dark} - the dark current of the detector, and n_{RN} - the read-out noise from the read-out integrated circuit (ROIC).

Fig.12 shows the evaluation of the Eq. (4) using the IR flux and source parameters from Table.8. A SNR > 10^3 can be achieved for integration times longer than 0.3 μs. For integration times longer than 20 μs the maximum well capacity is achieved and the detector will be saturated basically from the dark current of the detector and the synchrotron radiation flux to be measured. The performance becomes even better at higher photon energies than calculated here (<1000 cm^{-1}). The synchrotron flux increases and the beam emittance decreases with higher photon energies yielding to higher SNR for a given integration time.

In order to follow a process in time the spectra have to be acquired in series. The time past between two spectra collected successively determines the time resolution of the spectrometer. In addition, the ROIC of the FPA has to be able to allow a fast data transfer. For a 256 pixel linear array and a time resolution of 1 μs aimed pixel rates of 32 MHz are sufficient if the ROIC is divided into 8 channels.

To evaluate the performance of a time-resolved X-ray absorption experiment, we may consider a standard XAS measurement at the Fe *K* edge (7112 eV) where a total flux of $2.1*10^9$ photon/sec/0.1%b.w. is available in the same sample area.

If we define a S/N ratio we may evaluate the minimum acquisition time necessary to collect a spectrum in the dispersive geometry. We considered a typical XANES spectrum that starts from 50 eV below the edge to ~ 200 eV above the edge and from ~100 eV below the edge up to 800-1000 eV above the edge for an EXAFS acquisition. In the transmission dispersive mode X-ray absorption spectra are collected using a detector such as an ionization chamber before the sample and an array detector after the sample.

If we assume I_0 the flux before 1st ionization chamber and ζ the fraction of the photon intensity absorbed by the 1st ionization chamber, the measured value is $I_0\zeta$. After a sample of thickness x, the intensity will decrease to $I_t=I_0*(1-\zeta)*e^{-\mu_t x}$, where μ_t is the absorption coefficient of the sample. In a ideal transmission experiment all photons will be absorbed by the detector following the sample.

The ratio $r=I_0\zeta/I_t=\zeta/[(1-\zeta)*e^{-\mu_t x}]$ is the signal measured by the experiment. The goal is to maximize the accuracy in the variations of r induced by the small change of μ, the absorption coefficient of the material that is a function of the energy. Then, the real signal is the first order derivative of r respect to μ:

$$S=dr/d\mu_t = x * \zeta/[(1-\zeta)*e^{-\mu_t x}] \quad (5)$$

The statistical noise of this measurement can be estimated with the formula [29]:

$$\frac{S}{N} = x \bullet \sqrt{\frac{I_0}{(\frac{1}{\zeta} + \frac{e^{\mu_t x}}{1-\zeta})}} \quad (6)$$

so that when ζ=20%, $\mu_t x$=2.6 and we can achieve the maximum S/N ratio [29]. In practical cases, $\mu_t x$, i.e., the jump at the edge, has to be <1.5 and > 0.8. While XANES structures are typically intense features, an EXAFS oscillation ranges between 1% and 10% of the total signal [30]. As a consequence, to collect reasonable EXAFS spectra the noise has to be <1% of the signal. A S/N>150 that correspond to a noise of 0.67% of the total signal is typically suitable to collect good EXAFS spectra.

To collect a good spectrum we may assume that about 20% photons can be absorbed by the 1st ionization chamber (ζ=0.2) and that the reference homogeneous sample containing iron has a characteristic edge jump of 1.2 ($\mu_t x$=1.2). If the EXAFS range is defined from 7057 to 8000 eV around the iron *K*-edge (7112 eV) the optimum absorption thickness of a iron foil is

$$x = \frac{1}{\mu_{Fe}(8000eV) - \mu_{Fe}(7057eV)} = 5.1\ \mu m \quad (7)$$

(μ_{Fe}(7057 eV)= 419.163 cm^{-1} and μ_{Fe}(8000 eV, 15A^{-1}) = 2376.273 cm^{-1} as available from the McMaster Table). [31]

With the parameters ζ=0.2, x=5.1 μm and $\mu_t x$=1.2 and considering the optimal S/N=150, using the Eq.5 the minimum flux is 8x10^9 photon/sec/0.1% b.w./mm^2. Because the incident intensity on the sample is 3.36*10^{10} photon/sec/0.1% b.w./mm^2 we need about 240 ms to collect a spectrum at the Fe *K*-edge up to k~15 A^{-1} with S/N better than 150. A smaller range and a lower S/N ratio should allow faster acquisitions down to a few ms.

CONCLUSIONS

We present here the first optical layout of a combined Infrared and X-ray beamline to be built on a 3rd generation synchrotron facility for time-resolved concurrent/simultaneous IR and X-ray experiments whose 3D layout has been outlined in Fig.13. The X-ray and IR optical systems can be extracted from the same bending magnet and transported with two almost independent optical layouts. A specifically designed optical system, e.g., a condenser system, may allow to merge the two beams in order to fulfil a paraxial geometry at the sample location. Ray-tracing calculations showed that the x-ray system may allow to measure Fe *K*-edge XAS spectra in a large energy range (up to k~15 A^{-1}) within 240 ms with a S/N ratio better than 150 on sample area of 0.05-0.06 mm^2.

Spectra in the IR region could be simultaneously measured with a high S/N ratio due to the large brilliance available from a third generation synchrotron radiation source with an accumulated

current greater then 300 mA. Actually, in the mid-IR spectral range time resolved spectroscopy with a SNR > 10^3 and a time resolution of the order of μsec appears possible with the dispersive spectrometer here described.

These performances indicate that the IXSS beamline can make possible new and unique researches in different fields. Indeed, the combined optical layouts offer unique spectroscopy/microscopy opportunities for concurrent investigations of the electronic and vibrational structures in biological, materials science and many other scientific areas where physical/chemical processes occur [4)].

ACKNOWLEDGEMENTS

We gratefully acknowledge the support of the Italian Ministry Foreign Affairs in the framework of the 12th Executive Programme of Scientific and Technological Cooperation between the Italian Republic and the People's Republic of China. We sincerely acknowledge the SSRF facility that provided detailed information for the font-end beamline design. One of the authors (WX) thanks the Italian Ministry of Foreign Affair for financial support and acknowledge the hospitality of the LNF where a significant portion of this work has been performed. This work was partly supported by the Knowledge Innovation Program of the Chinese Academy of Sciences (KJCX2-YW-N42) A special thank is devoted to Manuel Sanchez del Rio, Qingxi Yuan and Lingyun Tang, Zeming Qi and Alessio Bocci and Paul Dumas for many useful discussions. This work was partly supported by the Knowledge Innovation Program of the Chinese Academy of Sciences (KJCX2-YW-N42).

REFERENCES

(1) http://www.esrf.eu/news/general/time-resolved-studies-feature-in-the-esrfnews/
(2) W. Bras, G.E. Derbyshire, D. Bogg, J. Cooke, M.J. Elwell, B.U. Komanschek, S. Naylor and A. Ryan, Science 267, 996 (1995).
(3) P. Innocenzi, L. Malfatti, T. Kidchob, S. Costacurta, P. Falcaro, M. Piccinini, A. Marcelli, P. Morini, D. Sali and H. Amenitsch, J. Phys. Chem. C 111, 5345 (2007)
(4) A. Marcelli, D. Hampai, Wei Xu, L. Malfatti and P. Innocenzi, Acta Phys. Pol. A 115, 489 (2009).
(5) H. Wende, Rep. Prog. Phys. 67, 2105-2181 (2004).
(6) C.R. Natoli, M. Benfatto, S. Della Longa and K. Hatada, J. Sync. Rad. 10, 26 (2003)
(7) F.C. Brown, P.L. Hartman, P.G. Kruger, B. Lax, R.A. Smith and G. Vineyard, *Synchrotron Radiation as a Source for the Spectroscopy of Solids*, NRC Solid State Panel Subcommittee Rep. (March, 1966).
(8) J.R. Stevenson, H. Ellis, and R. Bartlett, Appl. Optics 12, 2884 (1973).
(9) W. Duncan, G.P. Williams, Applied Optics 22, 2914-2922 (1983).
(10) J. Yarwood, T. Shuttleworth, J.B. Hasted, and T. Nanba, Nature 312, 742 (1984).
(11) T. Nanba, Y. Urashima, M. Ikezawa, M. Watanabe, E. Nakamura, K. Fukui and H. Inokuchi, Int. J. Infr. Mill. Wave 7, 1769 (1986).
(12) T. Nanba, Rev. Sci. Instrum. 60, 1680 (1989).

(13) A. Marcelli and P. Innocenzi, *A new beamline concept for fast IR and X-ray Simultaneous Spectroscopy*, Diamond User Meeting (Oxford, September 13-14, 2007)
(14) S. Pascarelli, O. Mathon, M. Munõz, T. Mairs and J. Susini, J. Sync. Rad. 13, 351 (2006).
(15) A.K. Freund, ESRF internal report: X-ray optics, Part 1 (1987).
(16) http://ssrf.sinap.ac.cn/english/.
(17) http://www.diamond.ac.uk/.
(18) http://www.ihep.ac.cn/bsrf/english/main/main.htm.
(19) M. Sanchez del Río and R.J. Dejus, *Synchrotron Radiation Instrumentation*, 8th International Conference on Synchrotron Radiation Instrumentation, eds. T. Warwick *et al*. (2004) AIP
(20) P. Dumas, F. Polack, B. Lagarde, O. Chubar, J.L. Giorgetta and S. Lefrançois, Infrared Phys. Technol. 49, 152 (2006).
(21) www.zemax.com.
(22) F. D'Acapito, F. Boscherini, A. Marcelli and S. Mobilio, Rev. Sci. Instrum. 63, 899 (1992).
(23) R.O. Hettel, Rev. Sci. Instrum. 73,1396 (2002).
(24) L.G. Parratt, Phys. Rev. 95, 359 (1954)
(25) A. Gibaud and S. Hazra, Current Science, 78, 1467 (2000)
(26) J. Headspith, J. Groves, P.N. Luke, M. Kogimtzis, G. Salvini, S.L. Thomas, R.C. Farrow, J. Evans, T. Rayment, J. S. Lee, W.D. Goward, M. Amman, O. Mathon and S. Diaz-Moreno, *The Nuclear Science Symposium Conference Record*, 2007. NSS '07. IEEE.
(27) E.N. Lewis, P.J. Treado, R.C. Reeder, G.M. Story, A.E. Dowrey, C. Marcott and I.W. Levin, Anal. Chem. 67, 3377 (1995).
(28) R.P.S.M. Lobo, J.D. LaVeigne, D.H. Reitze, D.B. Tanner, G.L. Carr, Rev. Sci. Instrum. 70, 2899 (1999)
(29) E.A. Stern and S. M. Heald, *X-Ray Absorption: Principles, Applications, Techniques of EXAFS, SEXAFS and XANES* (Wiley 1987).
(30) J.B. Hastings, (*Energy Citation Database BNL-28946; CONF-791139-1) Applications of EXAFS to Materials Science Conf., Boston, MA (USA)*, Nov.1979
(31) http://cars9.uchicago.edu/~newville/mcbook/
(32) *The lattice design of SSRF*, SSRF Internal Report 2004
(33) http://www.diamond.ac.uk/Home/Beamlines/B22/specs.html
(34) *URAP-GL-022BEPCII,* BSRF Internal Report 2006

Figures and Tables

TAB.1 Parameters of SSRF (Shangai), Diamond (Oxford) and BSRF (Beijing) facilities.

Electron parameters	SSRF [32]	Diamond [33]	BSRF [34]
Electron energy (GeV)	3.5	3	2.5
Electron current (mA)	300	500	250
Bending radius (m)	9.171	7.147	10.321
Bending magnetic field (T)	1.273	1.414	0.808
Critical energy (keV)	10.367	8.376	3.308
Energy spread	9.7×10^{-4}	7×10^{-4}	7.4×10^{-4}
Electron source size:			
Horizontal (cm)	0.0070	0.023	0.0623
vertical (cm)	0.0022	0.013	0.0535
Magnet length (m)	1.5	~1	<1.41
Magnet angle (deg)	9°	8°	7.8°

TAB.2 Optical parameters of a bent Si (111) crystal with a source divergence of 4 mrad

Element	Edge	Energy [eV]	Bragg angle [deg/mrad]	δE [eV]	R [m]	L [m]	Rocking curve [mrad]
Ti	K	4966	23.46/ 409.46	985.31	9.63	0.4526	0.0633
Mn	K	6539	17.60/ 307.17	1773.86	12.67	0.5956	0.0465
Fe	K	7112	16.14/ 281.72	2111.11	13.76	0.6468	0.0425
Cu	K	8979	12.72/222.01	3421.02	17.39	0.8175	0.0331
Sr	K	16104	7.05/123.09	11202.87	31.22	1.4671	0.0186 [fringes]
Pd	K	24350	4.66/81.29	25796.52	47.33	2.2247	0.0225 [fringes]
La	K	32660	3.47/60.57	46756.48	63.87	3.0018	0.0339 [fringes]

TAB.3 Optical parameters of the X-ray branch

Optics IXSS-X	M_{x1}	M_{x2}	*Slits2*	*Bent crystal*
Comments	Vertical focusing	Vertical steering/reflecting	Horizontal cut	Horizontal dispersion
Distance (from source point)	10 m	11 m	40 m	45 m
Incident angle	2.3 mrad	2.3 mrad	-	7.57°(132 mrad) @15keV
Figure	Cylindrical (elliptical) M=p/q=2	Plane	Rectangular H=4cm V=4cm	Elliptical M=p/q=22.5
Mirror and crystal length	1.2 m	1.0 m	-	30 cm
Mirror and crystal width	8 cm	8 cm	-	5 cm

TAB.4 Optical parameters of the IR branch

Optics IXSS-IR	M_{IR1}	M_{IR2}	M_{IR3}	M_{IR4}	M_{IR5}	M_{IR6}
Comments	extraction	focusing	Horizontal collimating	Vertical collimating	steering	condenser
Incident angle	45°	45°	45°	45°	41.905°	45°
Figure	Plane	Toroidal M=p/q= 0.44	Spherical	Spherical	Plane	Parabolic
Radius (cm)	-	Rt= 1251.84 Rs= 625.92	Rs= 2687.01	Rt= 5585.29	-	P=100
Mirror size LxV (cm)	15x20	20x24	20x24	20x24	20x24	20x24
Distance from the previous element (m)	5	0.77	38	0.75	3.11	7.04

TAB.5 Flux and wavenumber of the blackbody maximum at different temperature.

Temperature (K)	300	500	800	1000	1800
flux (photons/sec/0.1%b.w.)	$7.6x10^{6}$	$3.6x10^{7}$	$1.5x10^{8}$	$2.8x10^{8}$	$1.67x10^{9}$
wavenumber (cm^{-1})	539	995	1570	1709	3476

TAB. 6 Parameters of the dispersive IR spectrometer

Spectral range	Resolution at 1000 cm^{-1}	F/number	Number of spectral channels	Temperature of spectrometer optics	Efficiency
800-7000 cm^{-1}	2 cm^{-1}	6	256	77 K	50 %

TAB. 7 Data of the linear MCT FPA used for the performance estimation of the spectrometer

Cut-off	Dark current density @ 77 K	Pixel size	Well capacity	Read-out noise	Efficiency
800 cm^{-1}	$3.5x10^{18}$ $e^{-}/s/m^{2}$	40 μm	$5x10^{-7}$ e^{-}	500 e^{-} rms	1 e^{-}/photon

TAB. 8 IR synchrotron radiation parameters of the SSRF ring at 300 mA and at 1000 cm^{-1}.

Natural opening angle	Spectral flux@40 mrad horizontal acceptance	Source size	Emittance
17 mrad	$5.4x10^{13}$ photons/s/0.1%bdw	0.9 mm	$6.45x10^{-10}$ srm^{2}

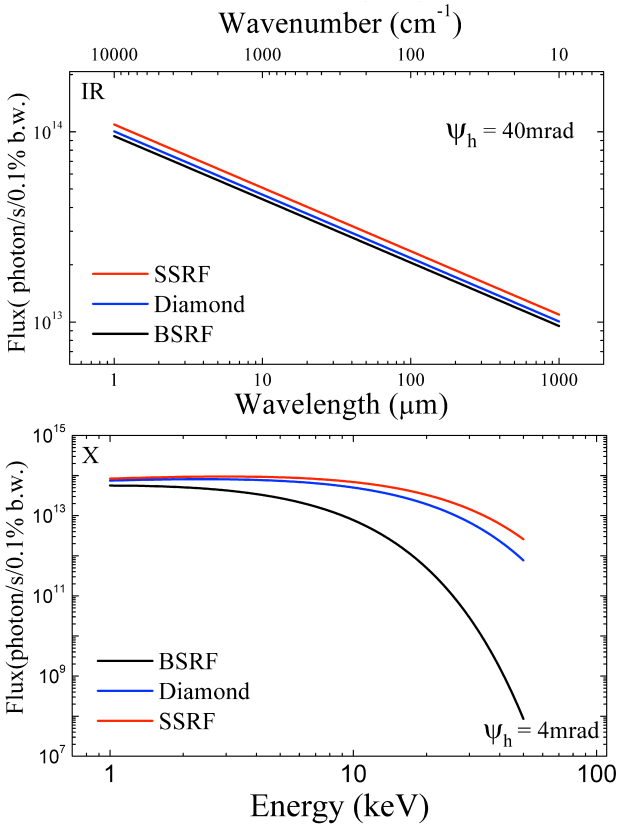

FIG. 1 Comparison of the photon fluxes at SSRF (300 mA), Diamond (500 mA) and BSRF (250 mA) in the IR (1-1000 μm) (top panel) and X-ray (1-40 keV) domain (bottom panel).

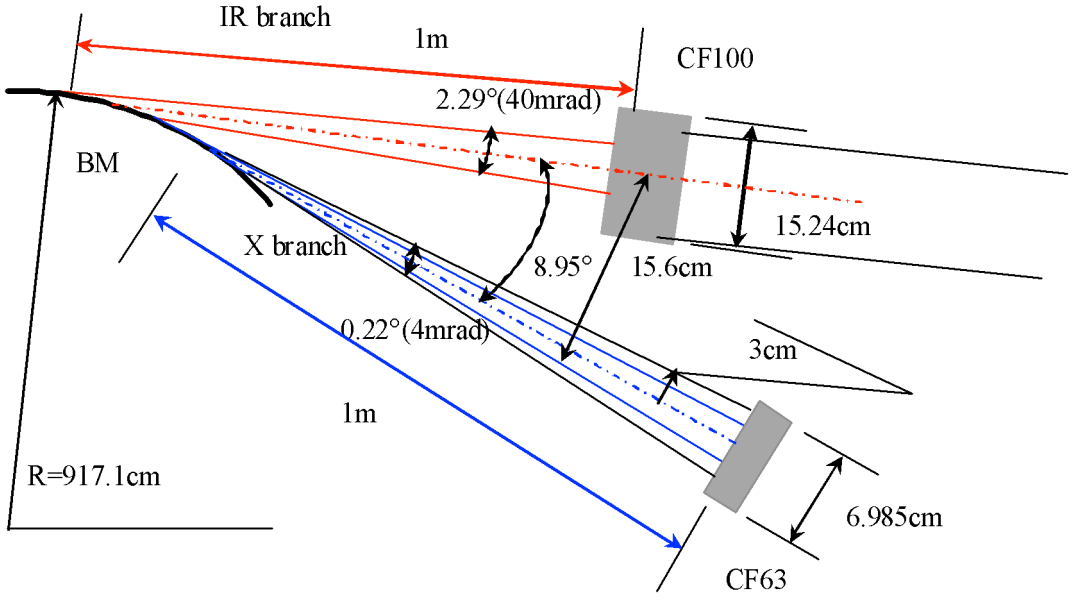

FIG. 2 The geometric layout of the extraction port for two IR and X-ray beams from a bending magnet at SSRF.

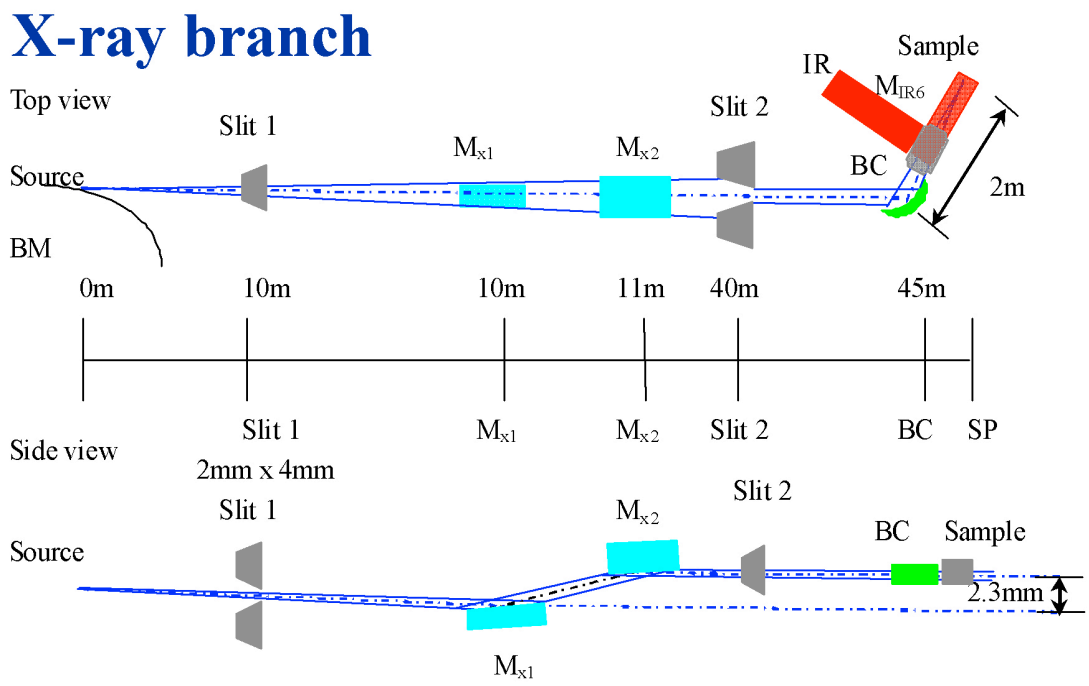

FIG.3 Top and side views of the layout of the IXSS-X ray optical system.

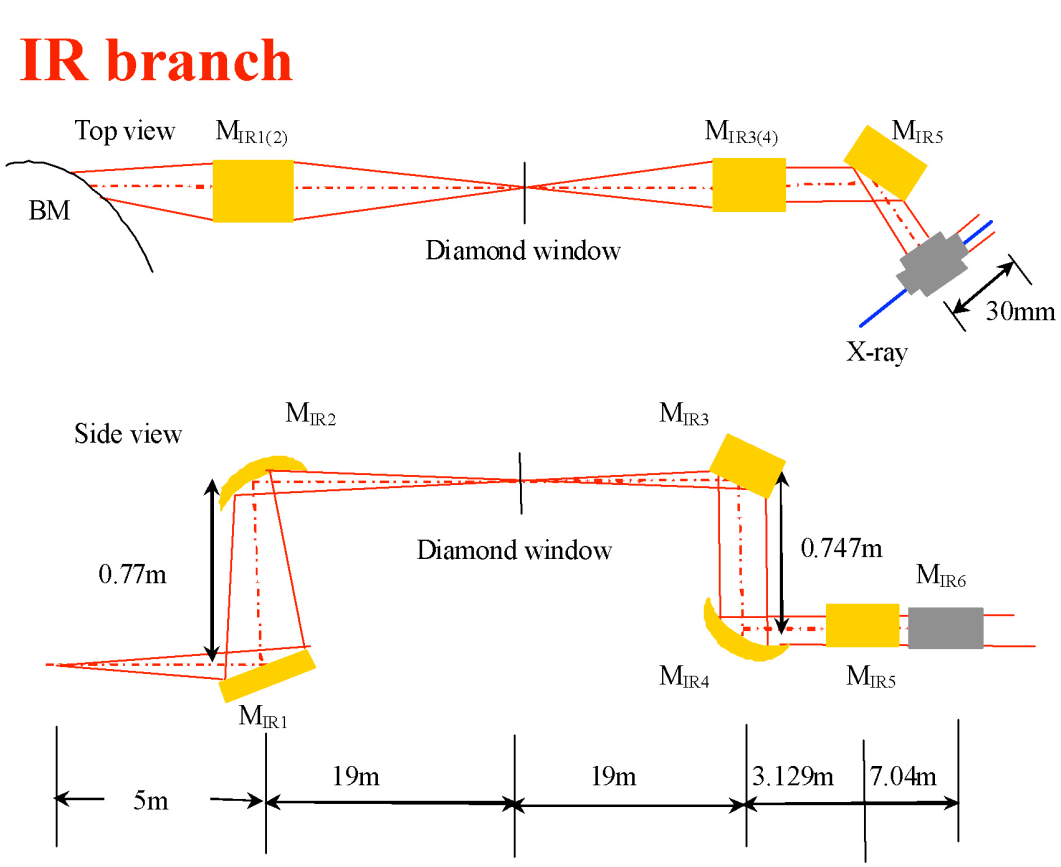

FIG.4 Top and side views of the layout of the IXSS-IR optical system.

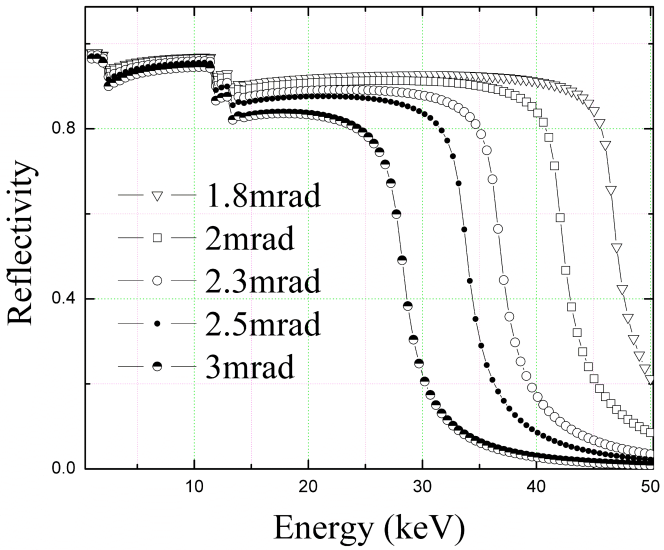

FIG.5 The reflectivity of a Pt coated mirror in the x-ray energy range as a function of the incidence angle.

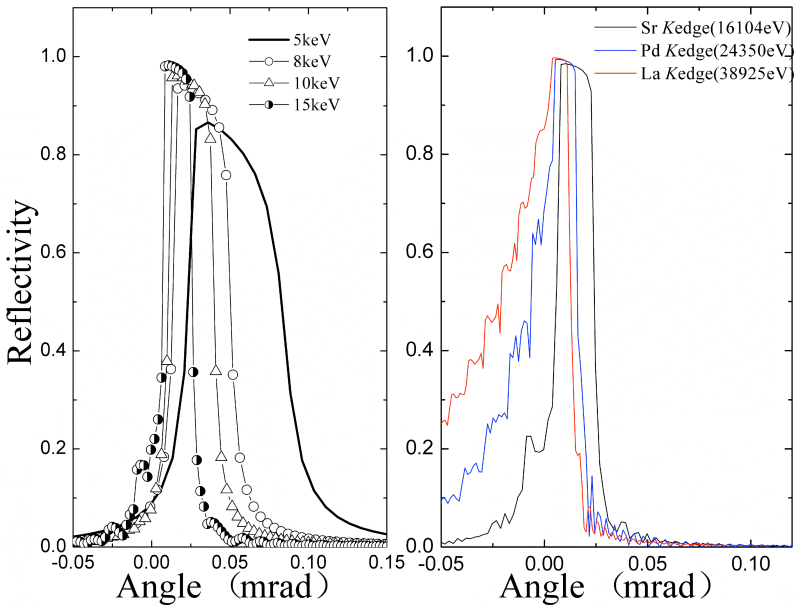

FIG.6 The reflectivity of a Si(111) bent crystal 0.7 mm thick working in the Bragg geometry, placed in the focusing condition p:q=45:2.

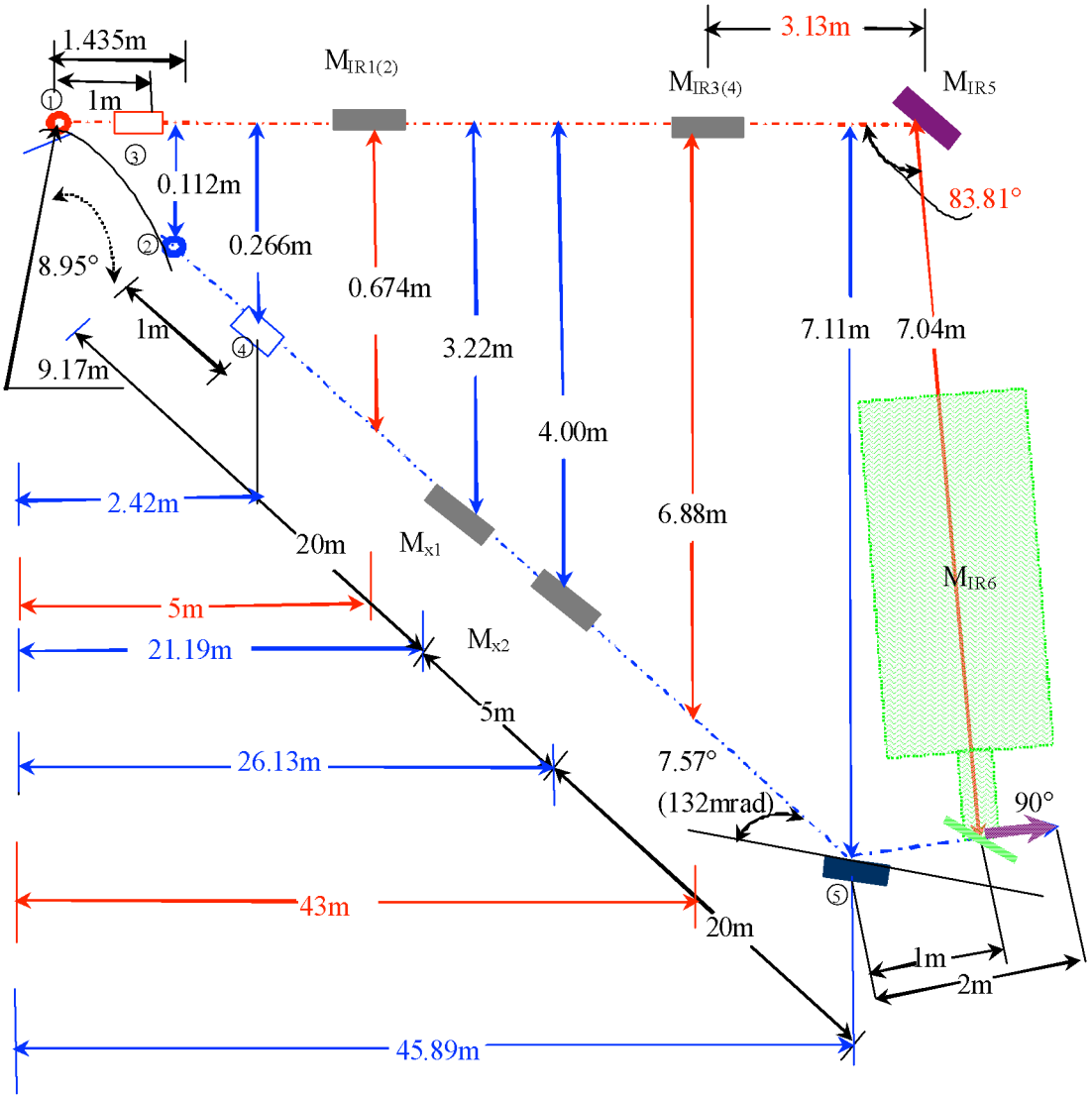

① IR emission point ② X-ray emission point
③ IR extraction aperture ④ X-ray extraction aperture
⑤ Bent crystal

FIG.7 Top view and optical parameters of the IXSS beam-line. The green area indicates the space of the condensing system M_{IR6}.

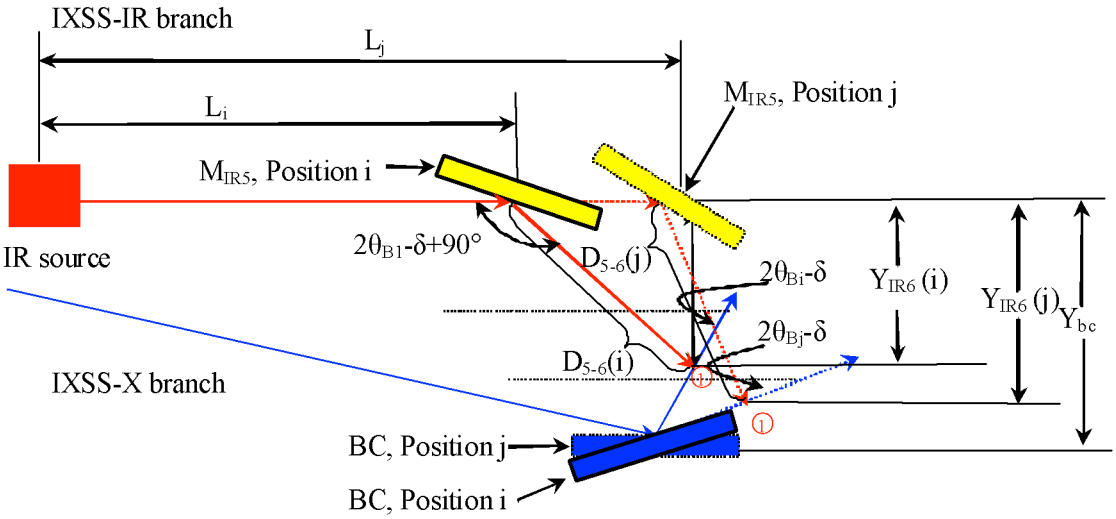

Y_{bc}=7.11m; the y coordinate of bent crystal

①: IR & X-ray crossing point

X_{bc}=45.89m; the x coordinate of bent crystal

$Y_{IR6}(i)=Y_{bc}-1*\sin(2\theta_{Bi}-\delta)$[m]; the y coordinate of IR& X-ray crossing point

$X_{IR6}(i)=X_{bc}+1*\cos(2\theta_{Bi}-\delta)$[m]; the x coordinate of IR&X-ray crossing point

$D_{5-6}(i)=Y_{IR6}/\cos(2\theta_{Bi}-\delta)$ [m]; the distance from the center M_{IR5} to the IR&X-ray crossing point

$Y_{IR5}=0$; y coordinate of M_{IR5}

$X_{IR5}=X_{bc}+1*\cos(2\theta_{Bi}-\delta)-Y_{IR6}*\tan(2\theta_{Bi}-\delta)$ [m]; x coordinate of M_{IR5}

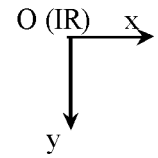

FIG.8 The combined mirror alignment of the X-ray and IR optics to collect XAS spectra. Here δ is the horizontal divergence of the X-ray beam.

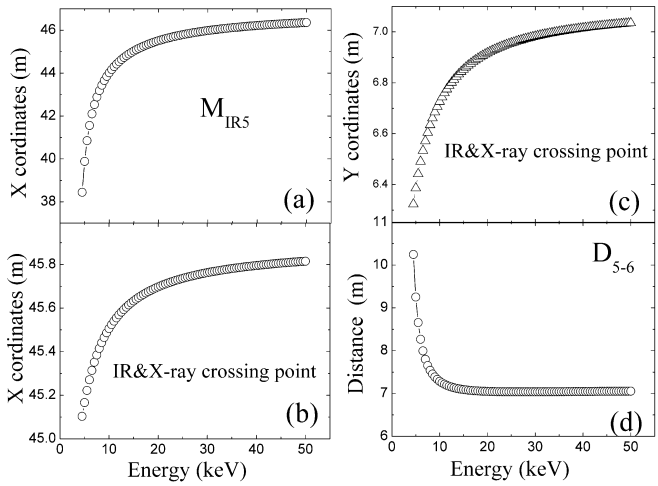

FIG. 9 (a) The energy dependent X coordinates of the IR mirrors M_{IR5} when the Y coordinate is set to zero; (b) the energy dependent X and (c) Y coordinates of the IR&X-ray crossing point (see Fig.8); (d) the distance D_{5-6} between M_{IR5} and the IR&X-ray crossing point vs. energy. The reference coordinate system whose origin is at the source point of the IR beam is shown in Fig.8. Actually, above 10 keV the distance D_{5-6} approaches asymptotically the value of 7 m.

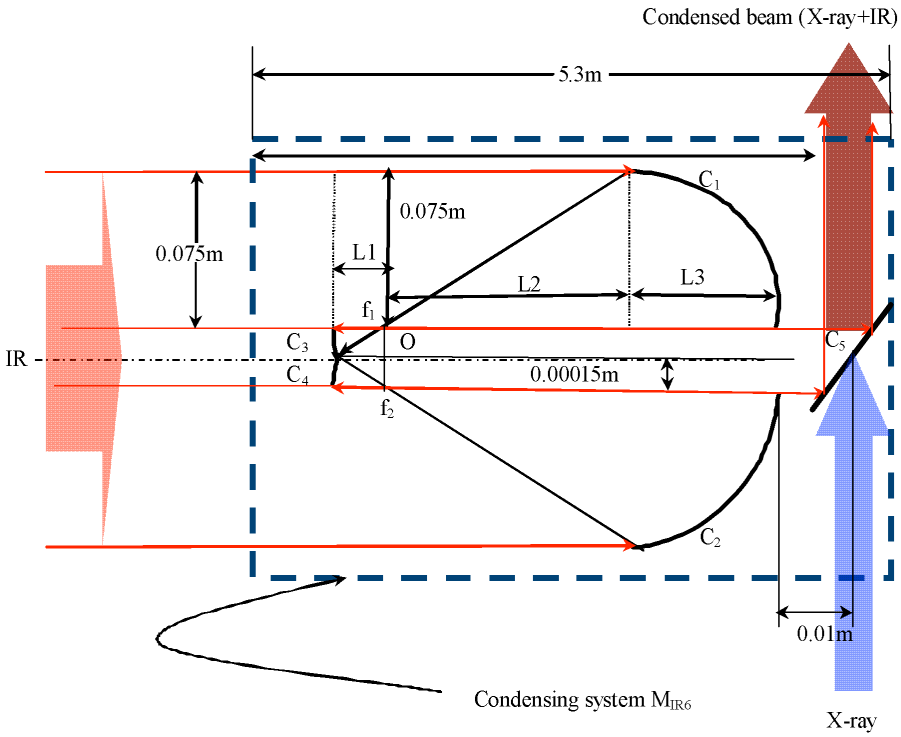

L1=0.01m; L2=4.99m; L3=0.1m
C_1 and C_2: primary parabolic mirror;
C_3 and C_4 : secondary parabolic mirror;
C_5: partially transmitting plane mirror

FIG.10 Schematic layout of the M_{IR6} condenser system. Dimensions are not to scale.

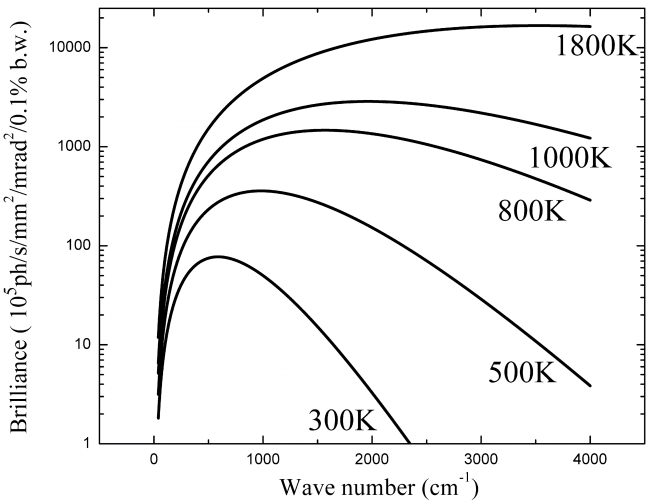

FIG.11 The brilliance of a black body source at different temperatures.

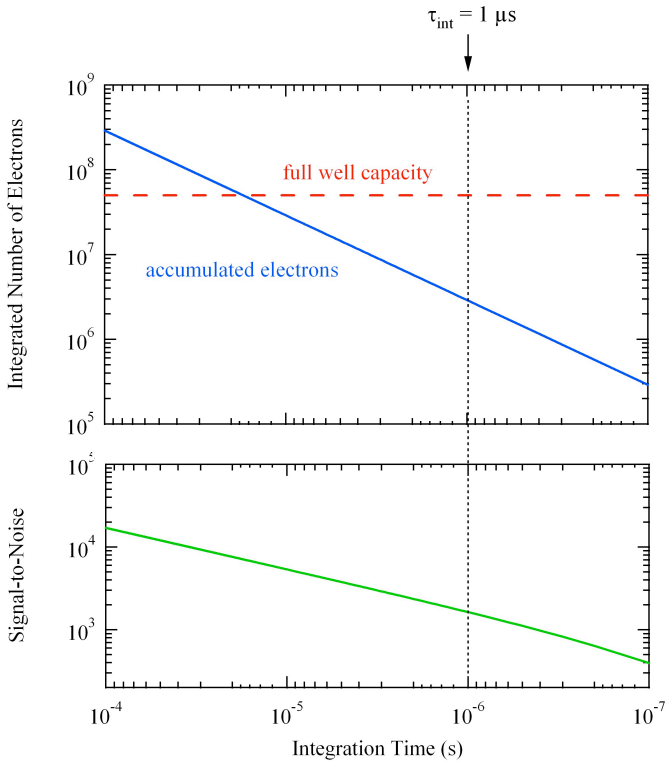

FIG. 12: In the top panel the total number of accumulated electrons vs. the integration time in comparison to the full well capacity. The expected SNR of the IR dispersive spectrometer at SSRF at 1000 cm^{-1} and with a spectral resolution of 2 cm^{-1} (bottom panel). The reference time resolution of 1 μs is marked with the vertical dotted line.

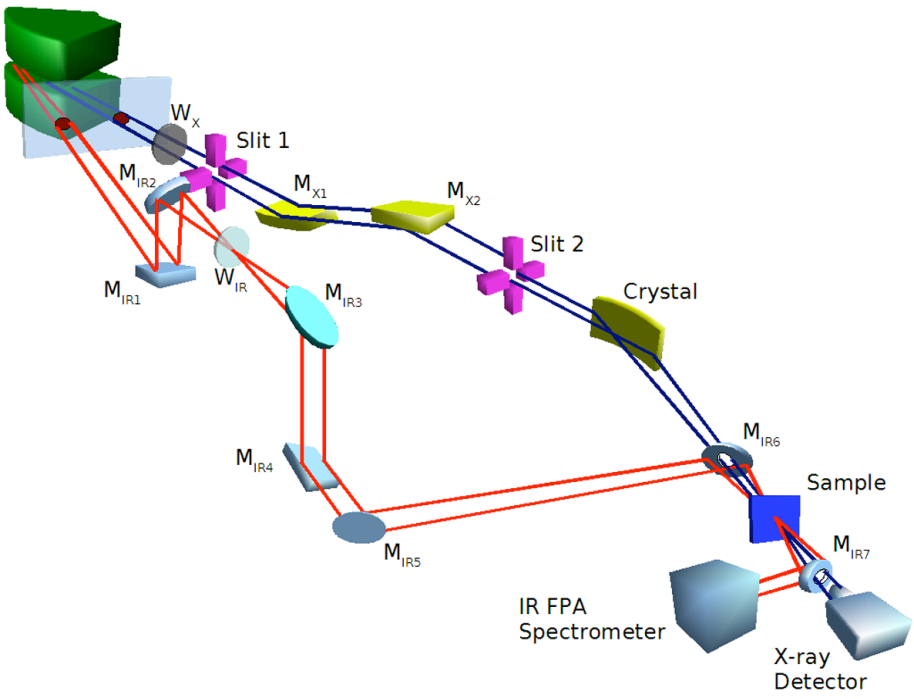

FIG.13 3D view of the schematic layout of the IXSS beamline.